Influence of Orography on Propagating Cyclones

Yuh-Lang Lin and David W. Hamilton
Department of Marine, Earth, and Atmospheric Sciences
North Carolina State University
Raleigh, North Carolina USA 27695-8208
and
Ching-Yuang Huang
Department of Atmospheric Science
National Central University
Chung-Li, Taiwan

1. Introduction

The mountains of Taiwan affect both the airflow and mesoscale weather systems impinging on the island significantly since two-thirds of this island country is covered by rugged terrain. The orographic feature which has the most significant impact on atmospheric systems is the Central Mountain Range (CMR) which runs through Taiwan in a NNE-SSW direction with a width of about 120 km, a length of about 300 km and an average height of 2 km (Fig. 1). The dominant peak of the CMR has a height of 3997m above the mean sea level. Since Taiwan is surrounded by oceans, it provides a unique environment for studying the orographic effects on particular mesoscale weather systems. When a typhoon impinges on Taiwan, its track, circulation, translation speed and strength are significantly affected by the CMR and proposes a challenging problem for weather forecasters in the country of Taiwan, as well as its neighboring countries, such as Japan, Korea, and China. Orographic influence on tropical cyclones in other parts of the world has also been investigated, such as in the northern Phillipines (Brand and Blelloch, 1973; Kintanar and Amadore, 1974) and in the Caribbean islands (Hebert, 1980).

According to the extensive observational studies of Wang (1980, 1989), when a typhoon impinges on the CMR at a certain angle, its track may remain continuous or become discontinuous (Fig. 2). In the first category, the typhoon may (a) simply continue its path over the mountain range, (b) deflect and stay for some time on the eastern side of the CMR, then pass over the mountain, or (c) have its upper-level center propagated over the mountain range, while its low-level center is deflected southward and disappears. In the second category, two or three secondary lows tend to form on the downstream side of the CMR, one of which then develops and replaces the center of the parent typhoon. Thus, the typhoon appears to jump over the mountain range. Based on these observations, Wang (1980) proposed that the typhoon is steered by the rear part of its own circulation and the basic flow when the front part of the circulation is blocked by the mountain range. Therefore, the typhoon center will be deflected toward the north (south) before (after) it passes over the CMR. However, this does not seem able to explain the southward (cyclonical) deflection shown in the example given in Fig. 3a. Using a primitive equation model, Chang (1982) found that the tropical cyclone's passage induces a mean cyclonic circulation around the mountain, which forces the cyclone to take a cyclonic track around the northern end of the island mountain. Even though Chang's numerical simulation results help improve the understanding of typhoon track deflection over Taiwan for northern-approaching typhoons, however, some central-approaching typhoons are deflected to the south on the upstream side of the mountain (Figs. 2 and 3). A northward upstream deflection for a westward propagating cyclone impinging on the central part of the Taiwan CMR has also been simulated by Bender et al. (1985, 1987) and Yeh and Elsberry (1993a) and observed by Tsai (1993) among others. The northward deflection is explained by enhanced blocking and deflection of the environmental flow. The low-level blocking of the typhoon has been observed using Doppler radar (Lee, 1993). Due to relatively coarse resolutions (60 km in Chang and 45 km in Yeh and Elsberry) and large mountains (240 km x 480 km in Chang and 320 km x 410 km in Yeh and Elsberry), it is difficult to compare their results directly with observations.

Chang (1982) also found that secondary vortex centers form in the lee trough, which may develop when they are in phase with the upper-level vortex center. He proposed that the horizontal advection of positive vorticity in conjunction with the leeside vortex stretching results in a mean positive vorticity around the mountain. Chan (1984) found that a definite link of local change in relative vorticity and tropical cyclone movement over a flat surface. On the other hand, Yeh and Elsberry (1993b) proposed that the vortex reorgnization downstream may occur as a downward extension from the upper-level remanants of the typhoon or as an upward growth of a low-level secondary vortex. In the second type, a new low-level center that is separate from the original vortex or the terrain-induced pressure trough becomes the center about which the tropical cyclone

reorganizes. However, the relationship between these two types of vorticity development remains to be explained. Using a shallow water numerical model, Smith and Smith (1993) found that vortex interaction with ideal topography results in a pair of trailing banners of vorticity which get wrapped up into the vortex as it drifts away. The potential vorticity production over the lee side when the cyclone approaches the mountain is explained by the transition from the irrotational flow regime to the regime of flow over mountain with wake. The new vorticity will be generated right on the lee side of the strongest wind normal to the mountain range in Chang's vorticity stretching mechanism, while it will be located to the left, if one faces downstream, of the strongest wind normal to the mountain range. This remains to be examined. Results of tank experiments (e.g., Pao, 1976; Hwang et al., 1977; Brand et al., 1982) may be compared with that of shallow water modeling simulations, such as Smith and Smith (1995), to help understand the basic dynamics of the formation of secondary vortices. However, a direct application of these types of approach, both tank experiment and shallow water numerical modeling, to the real atmosphere is still limited due to the assumptions made in these experiments and models, such as a free surface and the lack of stratification. It appears the simplicity of the shallow-water model and the potential vorticity thinking may be able to provide insight of the vortex dynamics and deserve further study.

Beside the track deflection, the circulation of a typhoon can be modified significantly by the mountain. Based on observational analysis, Wang (1980) proposed that the circulation is only modified slightly by the mountain range for typhoons with a continuous track, while it is modified significantly for typhoons with a discontinuous track (Fig. 3b). This seems to be consistent with nonlinear theories since typhoons with a continuous track have stronger winds associated with them, which tend to be more linear since the Froude number (U/Nh) is larger. It is noteworthy to mention, however, that the flow circulations associated typhoon near the CMR may become extremely complicated, such as the existence of upstream flow blocking and splitting and downstream hydraulic jumps, and warrent a further study.

As mentioned above, relatively weaker typhoons tend to dissipate or to produce secondary lows on lee side and their tracks appear to jump forward or rapidly across the island (Wang, 1980; Brand and Blelloch, 1974). It has been shown that the stationary low is produced by downslope wind through adiabatic warming for uniform flow over Taiwan (Sun et al., 1991; Lin et al., 1992). Both statistical analysis of observational case studies (Wang, 1980) and tank experiments (Pao, 1976; Hwang et al., 1977) have shown that the formation of secondary lows is determined by the incident angle of the typhoon circulation and the Reynolds number. The secondary low forms farther to the north on the west coast of Taiwan for a larger angle α, where α is defined as the wind direction at Pengchia-Yu, located at about (122°E, 25.5°N), before the typhoon impinges on Taiwan subtracted by the orientation direction of the CMR. In addition, these secondary lows may become either dynamically active or inactive. Using an empirical orthogonal function (EOF) analysis of 82 typhoons that impinges Taiwan for a 20-year period, Chang et al. (1993) demonstrated that formation of the secondary low over the western coast tends to occur only when the typhoon center is in a rather narrow zone over and upstream of the southeastern region of Taiwan. Chang's results are consistent with other observational analyses and tank experiments. However, it remains to be answered if weaker cyclone is a necessary condition for producing the leeside secondary lows.

Brand and Blelloch (1974) found an average intensity (maximum surface wind) decrease of over 40% and a distinct northward deflection as the typhoons approach the island with a southward deflection after their passage over the CMR. Chang (1982) proposed that diabatic processes tend to generate convergence to maintain the vorticity of the tropical cyclone. Using a numerical model, Bender et al. (1985) found that the typhoons fill much more rapidly in numerical simulations with a mountain included. The mountain range affects the decay rate through reduction in the supply of latent and kinetic energy into the storm circulation during, as well as after, passage of the storm over the mountain. The results show that the effect of the mountain range is an enhancement of heavy precipitation to the right of the storm track immediately after landfall, which is probably related to increased coastal convergence. As suggested by Chang, experiments with a prescribed cumulus heating, which sustains the vortex, may be carried out to provide more information on the role of latent heating.

In this study, we will adopt a primitive-equation numerical model with latent heating represented by prescribed heating to investigate the orographic influence on a propagtaing cyclone over an idealized topography and then applied to the real topography of Taiwan. The representation of cumulus heating by a prescribed heating has been used for studying the evolution of potential vorticty associated with hurricanes (e.g., Schubert and Alworth, 1987; Moller and Smith, 1994) and has been proved to be successful. This type of study will fill the gap between the shallow-water appraoch (modeling and tank experiment) and sophisticated primitive-equation modeling since the heating-induced vortex may be

regarded as a forced vortex. The numerical model will be described in section 2. In section 3, we will investigate the effects of an idealized topography on both westward and a northwesteard prapagating cyclones. A summary is given in section 4.

2. The Numerical Model

The North Carolina State University geophysical fluid dynamics model used in this study is based on a three-dimensional, hydrostatic, Boussinesq fluid system. The model has the following characteristics:

(a) The leapfrog scheme is used for time marching.

(b) A fourth-order centered difference scheme is used for horizontal space derivatives.

(c) A second-order centered difference is used for vertical space derivatives.

(d) The lower boundary condition is $\dot{\sigma} = 0$.

(e) The upper radiation boundary condition is approximated by a sponge layer (Klemp and Lilly, 1978).

(f) A zero gradient lateral boundary condition is applied, which allows gravity waves generated in the computational domain to propagate out of the lateral boundaries.

(g) A five-point numerical smoother (Shapiro, 1970) is applied at every time step in both the horizontal and vertical directions, while a three-point smoother (Asselin, 1972) is applied in time.

The details of the numerical model can be found in Weglarz (1994), Lin and Jao (1995) and Lin and Wang (1996). This model has been tested rigorously against Long's nonlinear solution of flow over mountains by Lin and Wang. The basic wind (U) is assumed to be independent of x, y, and σ in this study. The real topography, which cuts through the atmosphere without modifying the initial fields, is then introduced. The Brunt-Vaisala frequency associated with the basic flow is assumed to be 0.01 s^{-1} for all experiments discussed in this study. The Coriolis effects are included in the model by making an f-plane approximations. The reference Coriolis parameter f_o is set to 5.8×10^{-5} s^{-1}, since the center of Taiwan is located roughly at 23.5°N latitude. The flow is assumed to be inviscid in the physical domain (i.e. $\nu=0$ for $z \le 10$km). The upper third ($10<z \le 15$km) of the computational domain is the sponge layer. The vertical grid interval is 500m, while the horizontal grid interval in both x and y directions is 20 km. The total number of model grid points in the x, y, and z directions are 64x64x31, respectively. The time interval is 20s. The idealized bell-shaped topography is prescribed as

$$h(x, y) = \frac{h_m}{\left[x^2/a_x^2 + y^2/a_y^2 + 1\right]^{3/2}}, \qquad (1)$$

where h_m is the mountain height and a_x and a_y are mountain half-widths in x and y directions, respectively. In this study, we have adopted the values close to the Taiwan CMR, h_m=2.5 km, a_x=25 km, and a_y=75 km.

A number of simulations have been conducted in this study. All experiments are performed for 36 hours. During the first 12 hours, the flow is adiabatic (Q=0) and geostrophic adjustment processes have yielded a quasi-steady state flow over the mountains by the end of this time period.

At 12h, the prescribed cumulus heating is then activated to spin up the vortex. The cumulus heating then stays steady for the rest of the time integration and is advected downstream with the basic flow. The maximum cumulus heating rate is assumed to be 7.2 $Jkg^{-1}s^{-1}$, which is equivalent to 52 mm hr^{-1}. The prescribed cumulus heating rate is estimated by the integrated vertical column of the rate of latent heating

$$q(x,y,z) = \frac{Q_o}{\left(x^2/b^2+y^2/b^2+1\right)^{3/2}} \sin\left(\frac{\pi(z-z_b)}{z_t-z_b}\right), \quad \text{for } z_b \le z \le z_t \qquad (2)$$

where

Q_o = heating rate,
b = horizontal scale of the cumulus heating,
z_b = heating base (1 km)
z_t = heating top (10 km).

In this study, we have used: Q_o=7.2 J kg^{-1} s^{-1}, b=50 km, z_b=1 km, and z_t=10 km. Figure 4 shows the relative vorticity, vector wind, and pressure perturbation fields at the for a barotropic flow over an idealized topography after 24h. The vector wind field indicates that a significant portion of the low-level flow is split due to a low nonrotating Froude number (Fr=U/Nh), 0.4, and a large aspect ratio (h_m/a), 0.1. Upstream blocking is also evident from the vector field (Fig. 4b). Downstream of the mountain, a pair of cyclonic and anticyclonic vortices are also generated by the flow, similar to that simulated by Sun et al. (1991) and Lin et al. (1992). The high-low pressure couplet (Fig. 4c) is produced and consistent with mountain wave theories (e.g., Smith, 1979). The potential vorticity field shows that two banners of positive and negative vorticities are produced to the north and south of the mountain on the lee side, respectively. It will be discussed later that these secondary vorticity associated with wakes tend to interact with primary vorticity to affect the cyclone's track. From the vorticity field (Figs. 4a and c) and the vector wind field (Fig. 4b), the flow appears to fall into the regime of flow around the mountain with wake (Regime II, see Fig. 1 of Smith and Smith, 1995) since there exists hydraulic jump over the lee slope (Fig. 4c), instead of the regime of irrotational flow (Regime I of Smith and Smith). Thus, the downstream potential vorticity is not generated by the strengthening hydraulic jump. In addition, the potential vorticity is also generated upstream of the mountain, which may

affect the cyclone track upstream. The vector wind field also indicates that there exists vortex shedding, with a cyclonic vortex generated first, then an anticyclonic vortex, and at last a smaller-scale cyclonic vortex generated to the northwest of the mountain. This type of vortex shedding has also been predicted in a shallow water model (e.g., Schar and Smith, 1993b). At z=3 km (Figs. 4c and d), the flow is much less disturbed, while with the downstream vorticity banners more aligned with the basic wind.

Figure 5 shows the relative vorticity, vector wind, and pressure perturbation fields at 3 km for a cyclone induced by the prescribed heating (Eq. (8)) propagating in a barotropic flow over a flat surface after 24 h. The results indicate that the cyclone is able to maintain its integrity when propagating downstream with the basic flow. The vector wind has a maximum on its right front sector of the cyclone (Fig. 5a). This is consistent with observations (e.g. Wang, 1980). The flow fields are almost symmetric, but stronger, after 24 h.

3. Influence of an Idealized Topography on Propagating Cyclones

In this section, we will discuss two cases: (a) a westward cyclone impinges on an idealized north-south oriented mountain range, and (b) a northwestward cyclone impinges on an idealized mountain range oriented 15° from north.

a. Westward propagating cyclone over an idealized north-south oriented mountain range

Fig. 6 shows a case for a cyclone embedded in an easterly barotropic flow over an idealized, north-south oriented mountain. The primary cyclone is approaching the center of the mountain range. The parameters of the flow and mountain geometry are the same as those used in Figs. 4 and 5. At 24 h, the primary vortex is located far upstream of the mountain. A strong northerly wind is produced in between the mountain range and the vortex by blocking and channeling effects. Along the cross section of the strongest wind, e.g. y=80 km, most of the flow are able to go over the mountain (Fig. 7). Similar to the case of uniform flow over mountain (Fig. 4a), a banner of positive vorticity forms on the lee side of the mountain. The banner of negative vorticity is very weak wind since there exists either no or very wind normal to the southern part of the mountain. The vorticity generated by the mountain at this time is much weaker than that associated with the primary cyclone. At this time (24 h), the pressure field is dominated by the low associated with the primary cyclone. At 3 km, both the vorticity and pressure fields associated with the cyclone are almost unaffected by the mountain (Fig. 6).

When the cylcone propagates closer to the mountain, such as t=29 and 30 h, the surface vorticity field becomes asymmetric, with the maximum region concentrated near the mountain (Fig. 6). The vorticity maximum on the eastern slope is associated with the potential vorticity generated by the blocking, which is consistent with observations (e.g., Wang, 1980). The vorticity banner on the western slope becomes stronger and shifts southward to the central part, which is enhanced by the cyclonic flow associated with the primary cyclone. A small region of weak negative vorticity is produced in between the propagating cyclone and the downstream vorticity banner. At this stage, the surface vortex is still colocated with the primary low. The cyclone low is still symmetric, which indicates that it is still dominated by the prescribed latent heating. From the vertical cross section, it can be seen that the surface vorticity is retarded by the mountain (Fig. 7). The upper part of the cyclone, such as that higher than 6 km, is able to pass over the mountain without retardation. At 3 km, the vorticity field is affected slightly with its maximum region elongated in the zonal wind direction. This also happens to the low associated with the cyclone. Notice that there is not much low pressure perturbation generated at this level.

In the next 3 hours (31, 32 and 33 h), the potential vorticity generated by lee wakes, as can be seen from the vorticity banner, has a strong interaction with the potential vorticity associated with the propagating cyclone. During this stage, there exist two vortex centers. One is located on the eastern slope, while another one is located on the western slope. The vorticity maximum appears to move southward at 31 h, accelerates over to the western slope at y=-40 km at 32 h, and then moves northwestward (Fig. 8). The southward movement of the vorticity maximum upstream of the mountain at 31 h may be explained by the interaction of the potential associated with the primary cyclone over the eastern slope and the potential vorticity generated by the lee wake associated with the strenthening hydraulic jump (Fig. 7). The potential vorticity generation by the hydraulic jump is also evidenced by the vorticity and streamline fields shown at 33 h in Fig. 7. The generation of new potential vorticity is evidenced by the more intense and concentrated vorticity centers at 33 and 34 h (Fig. 6). This is similar to that found by Smith and Smith (1995) using a shallow water theory. However, it appears that the uniform flow over the mountain range is already in the regime of flow over a mountain with wake (Regime II, Fig. 1 of Schar and Smith, 1993a; Smith and Smith, 1995), instead of irrotational flow (Regime I). Thus, the potential vorticity generation may be associated with the strengthening of the internal hydraulic jump, instead of through regime transition. This may also enhance the vorticity stretching over the lee side. Chang (1982) has found that the vortex stretching is dominant at this stage from a vorticity

budget analysis. At 33 h, the internal hydraulic jump appears to be able to helps transport the upstream blocked vorticity over to the lee side of the mountain along the center line (y=0 km). This may help explain the downward extension of upper-level vorticity as found by Yeh and Elsberry (1993b). In addition, their upward growth of low-level vorticity can be explained by the potential vorticity generation associated with the internal hydraulic jump. Similar to the vorticity field, there exists 2 low pressure centers during this stage, one located over the eastern slope and the other located over the western slope (Fig. 6). However, the low center at 33 h is located to the north of undisturbed track (y=0). This is explained by the hydrostatically produced low pressure by the strong downslope wind through adiabatic warming on western slope at this time. The pressure ridge over the northeastern slope is produced by the hydrostatic mountain wave, which is consistent with mountain wave theory (e.g. Smith, 1979) and resembles the pressure pattern observed in the vicinity of Taiwan CMR (Wang, 1980; Fig. 3a). The behavior of vorticity maximum and low pressure center at 3 km are similar to those located at surface (Fig. 6). The disturbance is stronger than earlier times because it is very close to the mountain top, 2.5 km. The tracks of maximum vorticity and low centers at 3 km are similar to those at the surface, except that the maximum is located at about y=0 km, instead of at y=40 km.

After 34 h, the cyclone is resuming its orginal westward track and symmetric circulation (Figs. 6-8). The vorticity and low centers at both the surface and 3 km move much faster over the mountain peak (Fig. 8). This is consistent with other observational and numerical studies which have shown that the translational speed of the cyclone also tends to increase along with the deflection when it passes over Taiwan CMR (Brand and Blelloch, 1974; Wang, 1980; Chang, 1982; Yeh and Elsberry, 1993a). The surface vorticity center and low turns southward upstream of the mountain due to the upstream blocking. This result is different from those of Chang (1982) and Yeh and Elsberry (1993a,b) and may be explained by that our model has: (a) a finer resolution, (b) a more realistic mountain scale, (c) a more intense cyclone, and (d) lack of feedback to latent heating from upward motion over the upstream (eastern) slope. We hypothesize that factors (a)-(c) are more dominant than factor (d) since the strong upstream blocking would inhibit strong upslope upward motion. Notice that we use a spatial reoslution of 20 km, versus 60 km of Chang and 45 km of Yeh and Elsberry. In addition, we use a mountain scale of 100 km x 300 km (i.e., roughly $4a_x$ x a_y), versus 240 km x 480 km in Chang and 320 km x 410 km of Yeh and Elsberry. Their Rossby numbers are 2 to 3 times smaller, thus the flow will aquire more cyclonic vorticity and rightward turning. This may contribute to the upstream northward turning in their westward moving cyclones. This remains to be examined by using a more realistic parameterization of cumulus convection with the present model setting. The primary surface vortex moves to the south of the original westward track on the lee side at 32h due to the strong southwestward downslope wind. On the other hand, the surface low shifts to the north of the original westward track, which is influenced by the strong adiabatic warming associated with the downslope wind. The deflections of vorticity center and low on 3 km are less than those at the surface and resume their original westward tracks earlier due to less blocking and weaker downslope wind at this level, as expected. In fact, the southward upstream deflection has been observed. For example, the tracks of 1967 Typhoon Clara and 1971 Typhoon Nadine for continuous track cases (Wang, 1980; also see Fig. 2a) and the typhoon track given in Fig. 3. Our simulation of a northern impinging typhoon also shows a northern upstream deflection (not shown), similar to those predicted by Chang (1982) and Yeh and Elsberry (1993a,b).

b. Northwestward propagating cyclone over an idealized mountain range

Fig. 9 shows a case for a cyclone embedded in a southeasterly barotropic flow over an idealized mountain which is oriented 15° from north clockwise. The primary cyclone is approaching the southern part of the mountain range. The parameters of the flow and mountain geometry are the same as those used in the previous case. At 24h, the primary vortex is located at about 160 km to the southeast of the southern tip of the mountain. The surface flow is blocked by the mountain range on the upstream slope. There exists a stagnation point over the northeast upslope and a recirculated flow to the east of it. A lee cyclone, similar to those formed for a barotropic flow over CMR of Taiwan (e.g., Sun et al., 1991; Lin et al., 1992), can be found on the lee side of the mountain. The impinging flow splits on the upslope and go around the mountain, with the majority of fluid particles flowing southward. Similar to the easterly case (Fig. 6), a strong jet is produced in between the mountain range and the vortex. The flow field may be roughly described by a superposition of a divergence flow with the center located on the upslope, a strong cyclonic flow associated with the primary cyclone, and a weak drifting lee cyclonic flow on the lee side. Similar to the case of unifrom flow over a mountain (Fig. 4a), two banners of positive and negative vorticity are produced on the lee side of the mountain (Fig. 9). However, the vorticity generated by the mountain at this time is much weaker than that associated with the primary cyclone. At 24h, the major low

pressure perturbation is dominated by the primary low, while a weak low is produced on the lee slope. At 3 km, the vorticity and pressure fields are almost unaffected by the moutain.

During the next 2 hours (29 and 30 h), the cylcone propagates closer to the mountain and the shape of the surface vorticity becomes elongated in the northeast-southwest direction, due to the blocking of the mountain on the airflow (Fig. 9). The maximum vorticity is located at the south corner of the mountain range, where the strong northerly downslope wind meets the southeasterly wind associated with the forced cyclone. The wind field on the western side of the mountain range is similar to that at 24h except that the downslope wind becomes stronger and occupies almost all the western slope of the mountain. This also produced a cyclonic deflection of the vorticity center track (Fig. 11). The lee cyclone drifts slightly further downstream. A new banner of positive vorticity forms to the east of the mountain range, which appears to be produced by the interation of the downslope wind over the eastern slope associated with the divergent flow and the cyclonic flow associated with the primary cyclone. The lee slope low pressure perturbation is stationary, which indicates that it is formed by the downslope wind through adiabatic warming. The surface low associated with the primary cyclone still colocates with the surface vorticity center and is located over the southern slope. The pattern of this primary cyclone low is almost symmetric, unlike the northeast-southwest oriented vorticity maximum region. Similar to the vorticity center, the surface low center is deflected cyclonically, i.e. toward west from northwestward (Fig. 11). The banner of positive vorticity remains about the same as that at 24h, while a new banner of positive vorticity develops to the east of the mountain range. This new banner of positive vorticity is formed by the southeasterly wind associated with the cyclone and the divergent wind over the eastern slope of the mountain range. The surface pressure field is dominated by the primary low at the southern tip of the mountain range and the mountain-induced high-low couplet near the middle of the mountain range. The low pressure region over the lee slope is gaining its strength from the stonger downslope wind over the western slope. At 3 km, the vorticity maximum region is elongated in the northwest-southeast direction at 29 h and then split into two centers at 30 h, with the stronger vorticity center located over the upstream slope. The splitting process is caused by the stronger winds over the western slope. Notice that there exists only one vortex center or circulation center over the southern slope at both 29 and 30 h. The flow at 3 km is less affected by the mountain. However, the primary low is located at the southern slope, about the center of the two surface vorticity maxima at 30 h. In other words, the primary vorticity and low centers start to decouple at 30 h. From the vertical cross section at 30 h (Figs. 10a-b), most of the flow are able to pass over the mountain range and form a stronger hydraulic jump which may generate more potential vorticity over the lee side (Smith and Smith, 1995).

At 31 h, the surface primary vortex moves further westward around the southern tip of the mountain range anticyclonically. In the meantime, there are three lows generated over the lee slope of the mountain. These lows are related to the secondary lows observed in typhoons over the CMR of Taiwan (e.g., Wang, 1980). Both statistical analysis of observational case studies (Wang, 1980) and tank experiments (Pao, 1976; Hwang et al., 1977) have shown that the formation of secondary lows is determined by the incident angle of the typhoon circulation and the Reynolds number. Using emperical orthogonal function (EOF) analysis, Chang et al. (1993) showed that the formation of the secondary low over the western coast of Taiwan tends to occur only when the typhoon center is in a rather narrow zone over and upstream of the southeastern region of Taiwan. The present model results are consistent with their results. Therefore, the formation of secondary lows depends more on the impinging angle and landing location, rather than the strength of the cyclone. In other words, a typhoon with a discontinuous track, i.e. a weaker typhoon, is not a necessary condition for the formation of leeside secondary lows since the cyclone has the same strength as that in the previous case. This type of secondary lows do not occur in the case with easterly moving cyclones over a north-south oriented mountain range. *This appears to be due to the requirement of a strong wind blowing perpendicular to the central portion of the mountain range.* At 3 km, the northwest primary vortex develops further and becomes dominative, while the southeast one is still prominant (Fig. 9). The primary low over the lee slope, which is affected by the pressure perturbation generated by the downslope wind through adiabatic warming. Notice that the strongest downslope wind at this level is located near the central part of the mountain, compared to that located almost over the entire downslope at surface.

For the next 2 hours (32 and 33 h), the surface primary vortex keeps moving around the southern part of the mountain range. Two processes may be identified during this stage, (a) the interaction of primary and secondary vortices (33 h), and (b) generation of potential vorticity by the hydraulic jump which produces the local northern vorticity center as shown in 33 h (Figs. 9 and 10c). During the first process, these two vortices rotate cyclonically slightly and distort each other. This is similar to the finding of shallow water results of Smith and Smith (1995) and to the westward propagating cyclone case. The primary and secondary vortices merge eventually, as predicted by theory (Aref, 1983). The strong downslope wind

is shifted further to the northwestern slope. In the pressure field, it can be seen that the middle secondary low develops further and dominates the pressure field. The low pressure produced by the downslope wind is still evident over the lee slope at 33 h. At 3 km, northwest vorticity center develops further and propagated northwestward further downstream. The western slope is dominated by strong southerly wind, unlike the easterly downslope wind at surface.

During 34 and 35 h, similar to the easterly case, the cyclone is resuming its northwestward movement and symmetric circulation except that the vorticity center is located in the northern part of the vorticity banner. This vorticity maximum appears to be generated by the stronger easterly wind.

4. Concuding Remarks

In this study, a primitive-equation numerical model with latent heating represented by prescribed heating is adopted to investigate the orographic influence on a propagtaing cyclone over an idealized topography and then applied to the real topography of Taiwan. The findings are summarized as follows:

- In addition to the primary vorticity associated with the cyclone, potential vorticity may be generated by a strengthening internal hydraulic jump. This may enhance the vortex stretching. This is similar to the shallow water theory (Smith and Smith, 1995) except there exists no regime transition. The hydraulic jump appears to play a role in transporting the upstream blocked primary vorticity to the lee slope.

- Both downward extension from the upper-level vorticity and upward growth of a low-level vorticity are predicted by the present model, similar to those of Yeh and Elsberry (1993b). The downward extension of the upper-level vorticity is explained by the vorticity transport by the internal hydraulic jump, while the upward growth of a low-level vorticity is attributed to the potential vorticity generation associated with the strengthening hydraulic jump when the cyclone is passing over the mountain.

- The primary and secondary vortices rotate with each other cyclonically and eventually merge when they propagate further away from the mountain range. The primary vorticity maximum region may become elongated, and even split into two centers, due to upstream blocking, and severe downslope wind.

- The low-level vorticity and low centers move much faster over the mountain peak. The surface vorticity center and low turns southward upstream of the mountain due to the upstream blocking and channeling effects and the adiabatic warming associated with downslope wind, respectively. The primary surface vortex shifts to the south of the original westward track on the lee side once the upper-level center moves over the mountain, due to the strong southwestward downslope wind. On the other hand, the surface low shifts to the north of the original westward track, which is influenced by the strong adiabatic warming associated with the downslope wind. The deflections of vorticity and low centers at 3 km are much weaker than those at surface and resume their original tracks earlier due to less blocking and weaker downslope wind at this level. Some southward upstream deflection typhoons have also been observed by Wang (1980).

- Multiple low centers form over the lee slope in a northwestward propagating cyclone impinges the mountain range. These low centers are produced by strong downslope wind which occupies almost the entire western slope since the impinging angle of the cyclone provides more flow perpendicular to the mountain range. Therefore, the formation of secondary lows depends more on the impinging angle and landing location, rather than the strength of the cyclone. In other words, a typhoon with a discontinuous track, i.e. a weaker typhoon, is not a necessary condition for the formation of leeside secondary lows. This appears to be due to the requirement of a strong wind blowing perpendicular to the cerntal portion of the mountain range.

Acknowledgments Discussions with Dr. R. B. Smith are highly appreciated. The author would like to thank Dr. R. P. Weglarz and T.-A. Wang for their help in developing the numerical model. This work is partially supported by the NSF Grant #ATM-9224595.

References

Aref, H., 1983: Integrable, chaotic and turbulent vortex motion in two-dimensional flows. Ann. Rev. Fluid Mech., **15**, 345-389.

Asselin, R., 1972: Frequency filter for time integration. Mon. Wea. Rev., **100**, 487-490.

Bender, M. A., R. E. Tuleya, and Y. Kurihara, 1985: A numerical study of the effect of a mountain range on a landfalling tropical cyclone. Mon. Wea. Rev., **113**, 567-582.

Bender, M. A., R. E. Tuleya, and Y. Kurihara, 1987: A numerical study of the effect of island terrain on tropical cyclones. Mon. Wea. Rev., **115**, 130-155.

Brand, S., and J. W. Blelloch, 1973: Changes in the characteristics of typhoons crossing the Philippines. J. Appl. Meteor., **12**, 104-109.

Brand, S., and J. W. Blelloch, 1974: Changes in the characteristics of typhoons crossing the island of Taiwan. Mon. Wea. Rev., **102**, 708-713.

Brand, S., J. C. Herb, J. C. Woo, J. J. Lou and M. Danard, 1982: Mesoscale effects of topography on tropical

cyclone-associated surface winds. Pap. Meteor. Res., **5**, 37-49.

Chan, J. C.-L., 1984: An observational study of the physical processes responsible for tropical cyclone motion. J. Atmos. Sci., **41**, 1036-1048.

Chang, C.-P., T.-C. Yeh, and J. M. Chen, 1993: Effects of terrain on the surface structure of typhoons over Taiwan. Mon. Wea. Rev., **121**, 734-752.

Chang, S. W.-J., 1982: The orographic effects induced by an island mountain range on propagating tropical cyclones. Mon. Wea. Rev., **110**, 1255-1270.

Hebert, P. J., 1980: Atlantic hurricane season of 1979. Mon. Wea. Rev., **108**, 973-990.

Hwang, R. R., H. P. Pao, and S. T. Wang, 1977: Laboratory study of the effects on typhoons when encountering the mountains of Taiwan Island. Academic Sinica, Taipei, Taiwan.

Kintanar, R. L., and L. A. Amadore, 1974: Typhoon climatology in relation to weather modification activities. WMO, No. 408, WMO, Secretariat: CP 5, CH-1211, Geneva 20, Switzerland.

Klemp, J. B., and D. Lilly, 1978: Numerical simulations of hydrostatic mountain waves. J. Atmos. Sci., **35**, 78-107.

Lee, C.-S., 1993: The effects of Taiwan topography on landfall typhoons. Proc. Int'l Workshop on Mesoscale Research and TAMEX Program Review, 138-143, April 26-30, Taipei, Taiwan.

Lin, Y.-L., 1993: Orographic effects on airflow and mesoscale weather systems over Taiwan. Terr. Atmos. Ocean, **4**, 381-420.

Lin, Y.-L., and I-C. Jao, 1995: A numerical study of flow circulations in the Central Valley of California and formation mechanisms of the Fresno eddy. Mon. Wea. Rev., **123**, 3227-3239.

Lin, Y.-L., and T.-A. Wang, 1996: Flow regimes and transient dynamics of two-dimensional stratified flow over an isolated mountain ridge. J. Atmos. Sci., in press.

Lin, Y.-L., N.-H. Lin, and R. P. Weglarz, 1992: Numerical modeling studies of lee mesolows, mesovortices, and mesocyclones with application to the formation of Taiwan mesolows. Meteor. Atmos. Phys., **49**, 43-67.

Long, 1954: Some aspects of the flow of stratified fluids. II. Experiments with a two fluid system. Tellus, **6**, 97-115.

Shapiro, 1970: Smoothing, filtering, and boundary effects. Rev. Geophys. and Space Phys., **8**, 359-387.

Moller, J. D., and R. K. Smith, 1994: The development of potential vorticity in a hurricane-like vortex. Quart. J. Roy. Meteor. Soc., **120**, 255-1265.

Schär, C., and Smith, R. B., 1993a: Shallow-water flow past isolated topography. Part I: Vorticity production and wake formation. J. Atmos. Sci., **50**, 1373-1400.

Schär, C., and R. B. Smith, 1993b: Shallow-water flow past isolated topography. Part II: Transition to vortex shedding. J. Atmos. Sci., **50**, 1401-1412.

Schubert, W. H., and B. T. Alworth, 1987: Evolution of potential vorticity in tropical cyclones. Quart. J. Roy. Meteor. Soc., **113**, 147-162.

Smith, R. B., 1979: The influence of mountains on the atmosphere. Adv. in Geophys., vol. **21**, B. Saltzman (ed.), Academic Press, 87-230.

Smith, R. B., and D. F. Smith, 1993: Pseudoinviscid wake formation by mountains in shallow-water flow with a drifting vortex. J. Atmos. Sci., **52**, 436-454.

Sun, W.-Y., J. D. Chern, C.-C. Wu, and W.-R. Hsu, 1991: Numerical simulation of mesoscale circulation in Taiwan and surrounding area. Mon. Wea. Rev., **119**, 2558-2573.

Tsay, C.-Y., 1993: Orography effects on the structure of typhoons: Analyses of two typhoons crossing Taiwan. TAO, **5**, 313-333.

Tuleya, R. E., and Y. Kurihara, 1978: A numerical simulation of the landfall of tropical cyclones. J. Atmos. Sci., **35**, 242-257.

Wang, S.-T., 1980: Prediction of the movement and strength of typhoons in Taiwan and its vicinity. Res. Rep. 018, Taiwan National Science Council, Taipei, Taiwan. (in Chinese)

Wang, S.-T., 1989: The characteristics of typhoon wind field and methods of gust wind prediction in Taiwan. National Science Council Tech. Rep., 77-58. Taipei, Taiwan, 94pp.

Weglarz, R. P., 1994: Three-dimensional geostrophic adjustment of rotating homogeneous and continuously stratified atmospheres with application to the dynamics of midlatitude jet streaks. Ph.D. dissertation, North Carolina State University, NC, 414pp.

Yeh, T.-C., and R. L. Elsberry, 1993a: Interaction of typhoons with the Taiwan orography. Part I: Upstream track deflections. Mon. Wea. Rev., **121**, 3193-3212.

Yeh, T.-C., and R. L. Elsberry, 1993b: Interaction of typhoons with the Taiwan topography. Part II: Continuous and discontinuous tracks across the island. Mon. Wea. Rev.,**121**, 3213-3233.

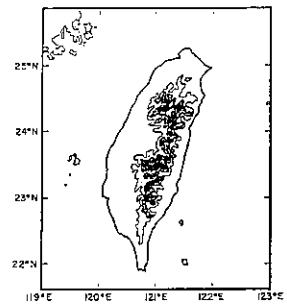

Fig. 1: Taiwan topography. Contoured shaded regions indicate elevations of every 1000 m.

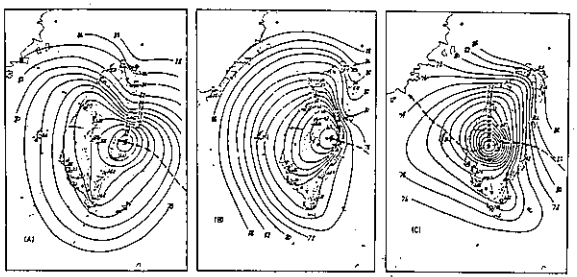

Fig. 3a

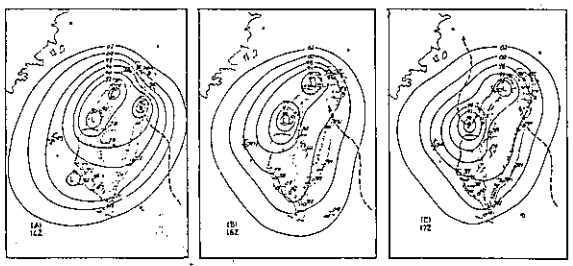

Fig. 3b

Fig. 3: (a) Flow circulations associated with a typhoon which has a continuous track, and (b) Flow circulations associated with a typhoon which has a discontinuous track. (after Wang, 1980)

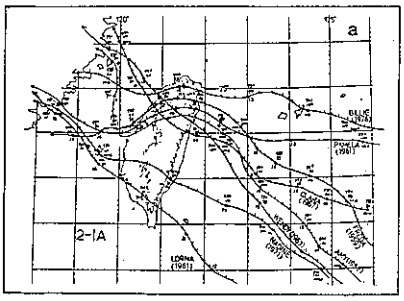

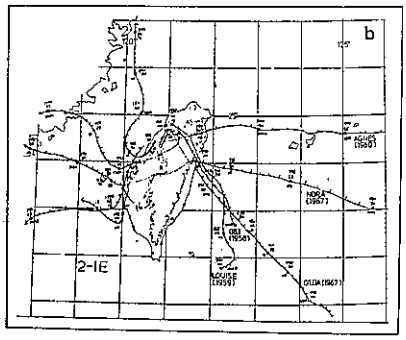

Fig. 2: Two types of typhoon tracks: (a) continuous and (b) discontinuous. (after Wang, 1980)

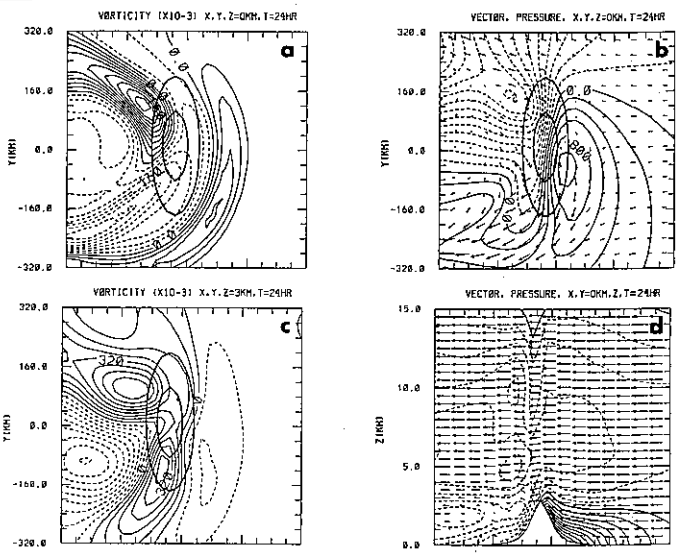

Fig. 4: (a) Relative vorticity at surface, (b) perturbation pressure and vector wind at surface, (c) relative vorticity at 3 km, and (d) pressure perturbation and vector wind at y=0 km for a barotropic flow over an idealized topography without cyclone after 24h.

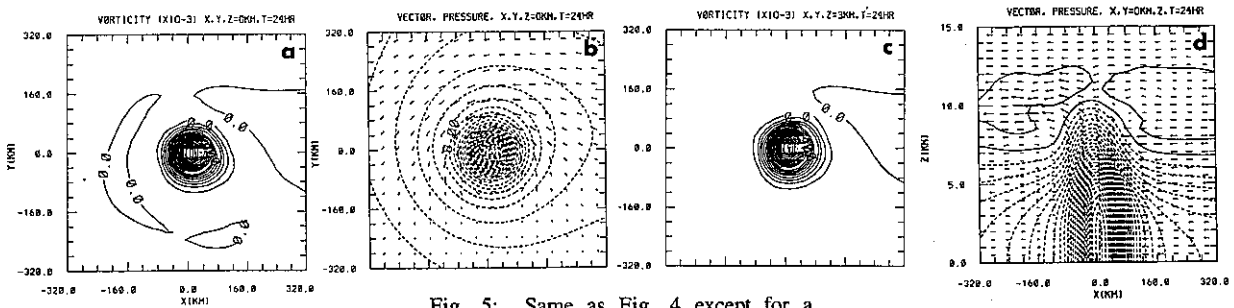

Fig. 5: Same as Fig. 4 except for a cyclone induced by the prescribed heating (Eq. (8)) propagating in a barotropic flow over a flat surface after 24h.

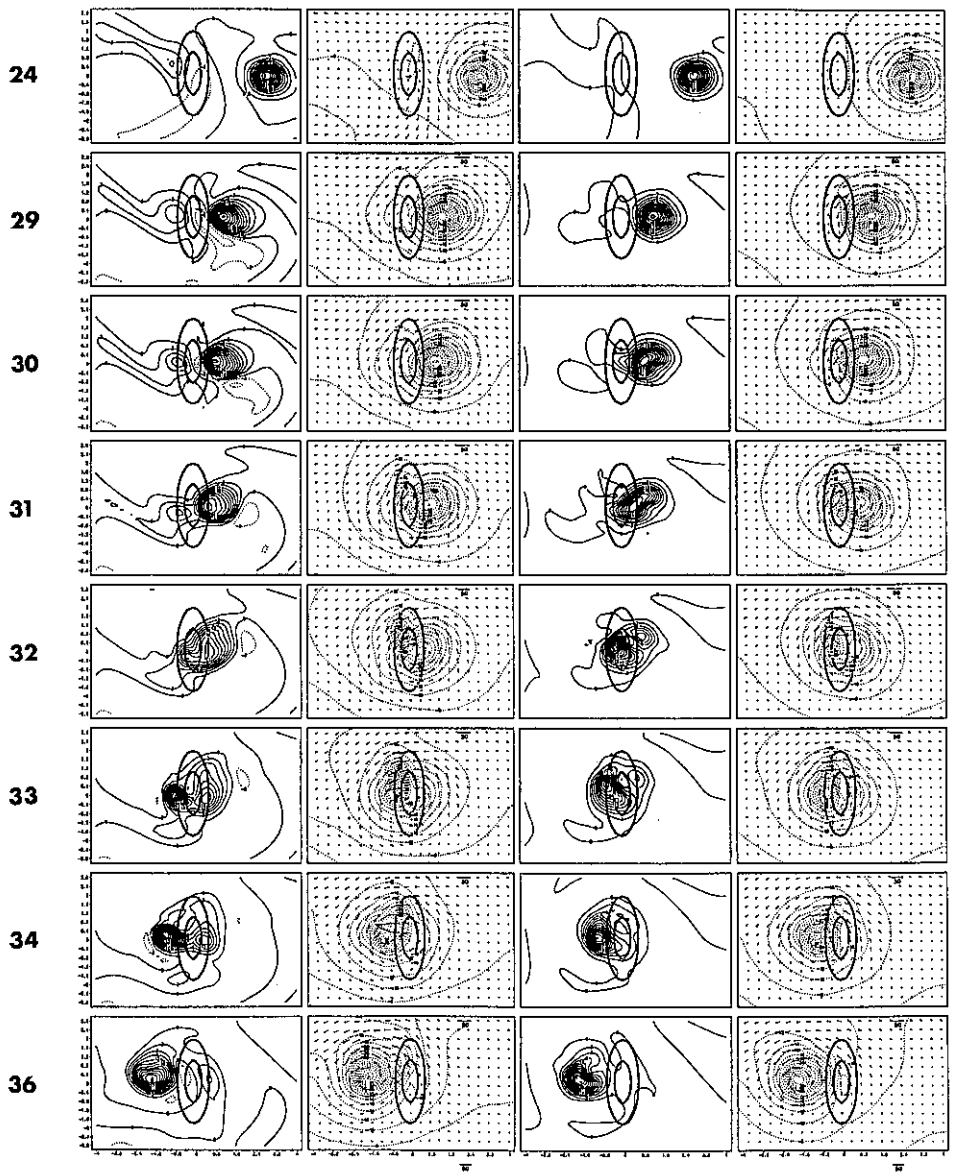

ζ'(sfc) p'(sfc) ζ'(3km) p'(3km)

Fig. 6: Relative vorticity fields (1st and 3rd columns) and pressure (2nd and 4th columns) at surface (1st perturbation and vector wind fields and 2nd columns) and at 3 km (3rd and 4th columns) for a cyclone embedded in an easterly flow over an idealized topography. Times shown are 24, 29, 30, 31, 32, 33, 34, and 36 h as indicated.

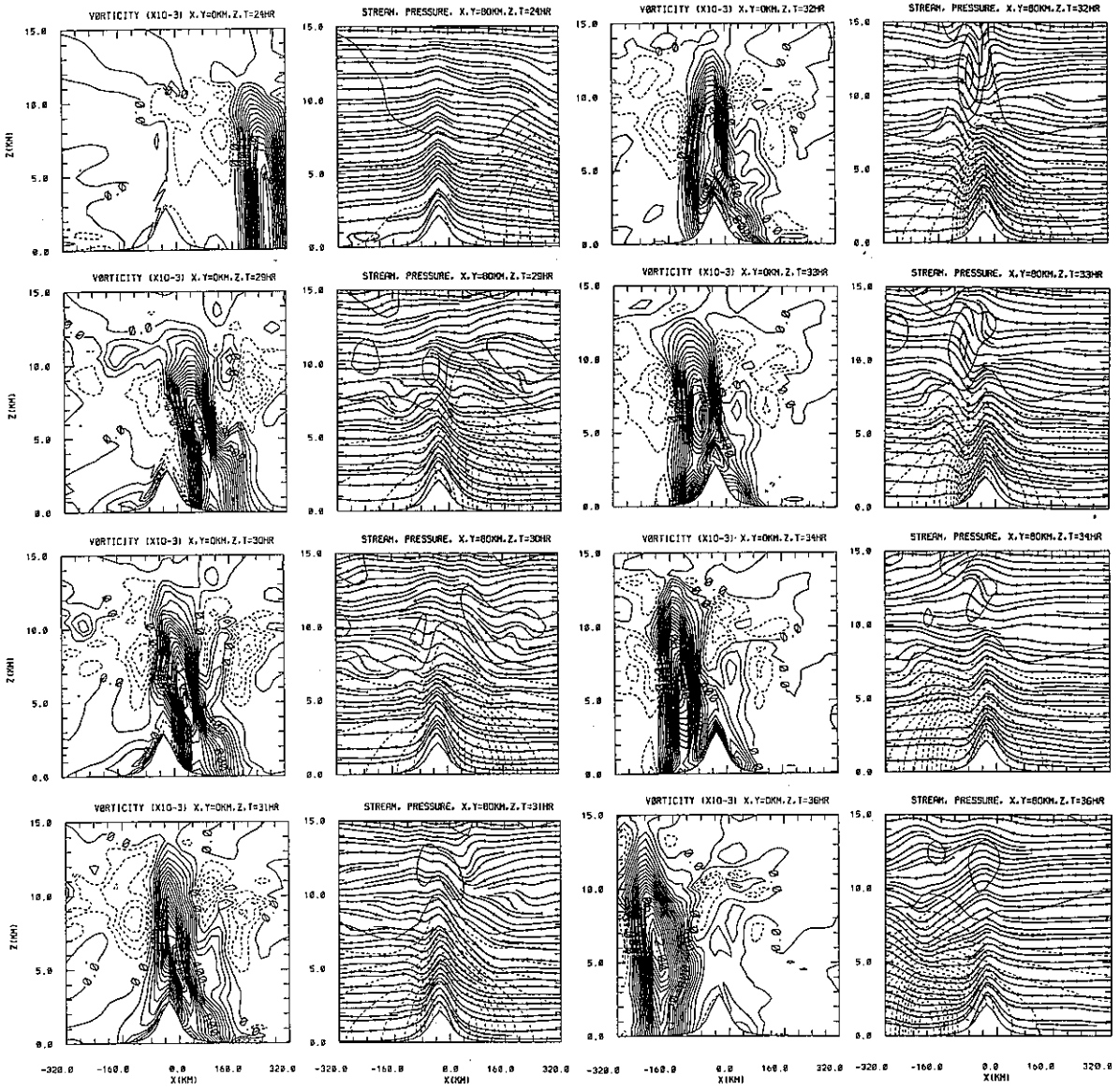

ζ' p' ζ' p'

Fig. 7: Vertical cross sections of relative vorticity (left panels) and pressure perturbation and streamlines (right panels) for a cyclone embedded in an easterly flow over an idealized topography at 24, 29, 30, 31, 32, 33, 34, and 36 h.

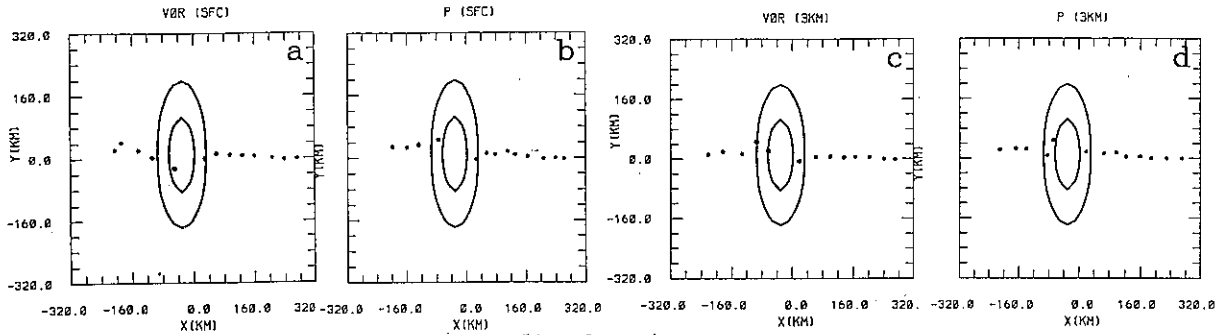

Fig. 8: Tracks of (a) surface vorticity center, (b) surface low, (c) vorticity center at 3 km, and (d) low at 3 km from 24 to 36 h.

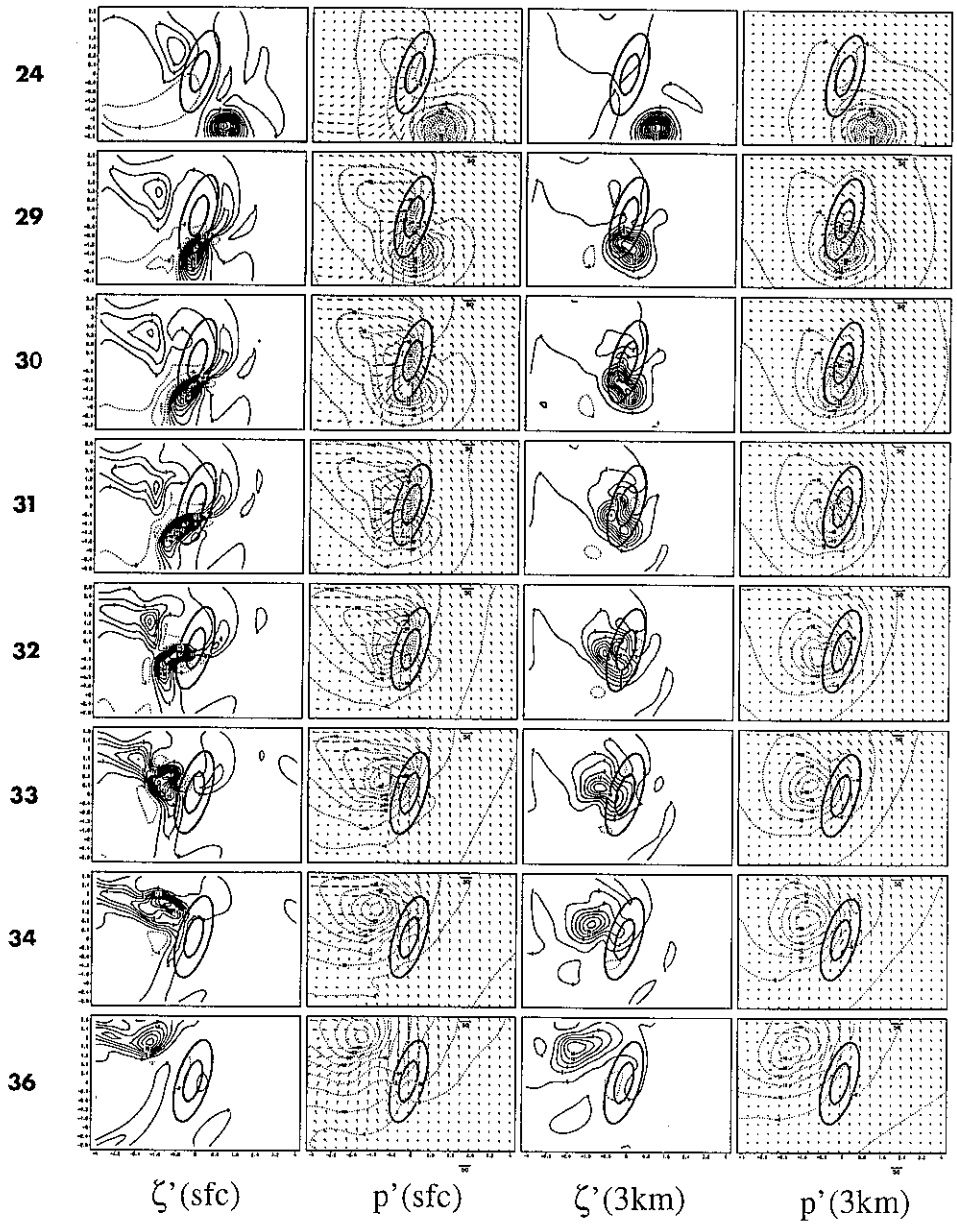

Fig. 9: Same 6 except for a southeasterly barotropic flow over an idealized topography oriented 15° from north clockwise.

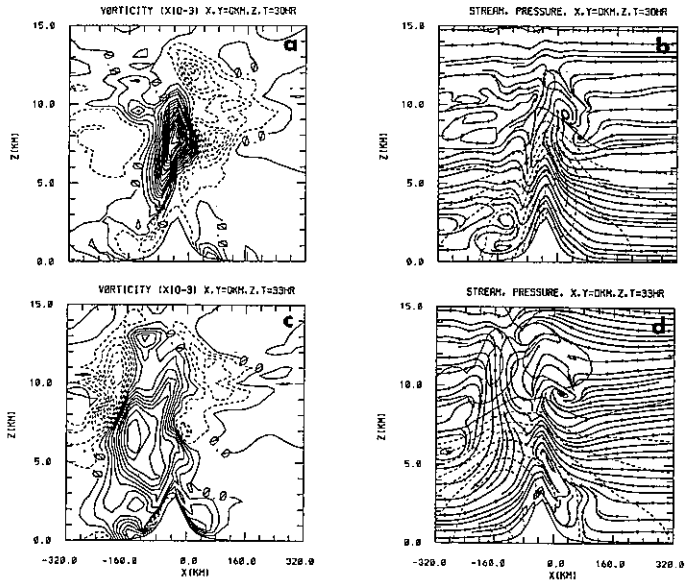

Fig. 10: Similar to Fig. 7 except for a southeasterly barotropic flow and only 30 and 33 h are shown.

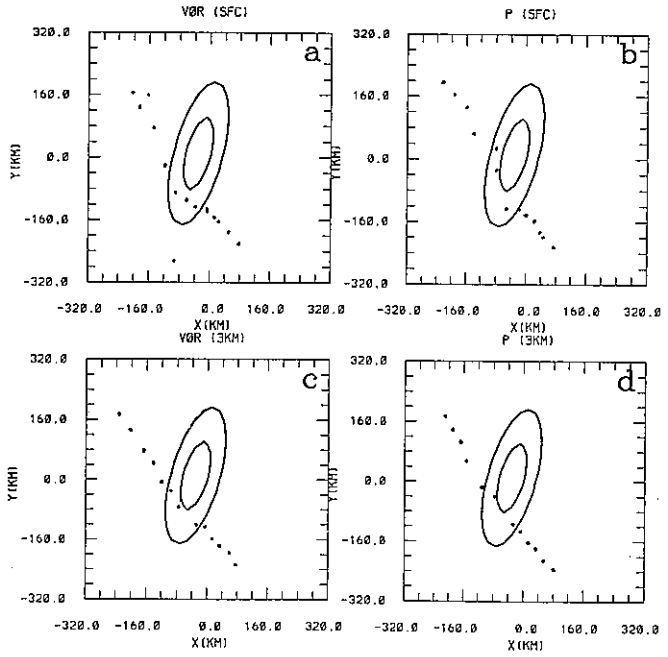

Fig. 11: Same as 8 except for a southeasterly barotropic flow.